VOL. 18, NO. 10, MAY 2023 ISSN 1819-6608
ARPN Journal of Engineering and Applied Sciences

www.arpnjournals.com

# EXPERIMENTAL AND NUMERICAL ANALYSIS OF RESIDUAL COMPRESSION STRENGTH AFTER LOW-VELOCITY IMPACT OF CARBON/EPOXY COMPOSITE PLATE

H. Syamsudin[1], M. G. Suada[1] and H. Romadon[2]
[1]Lightweight Structure Research Group, Faculty of Mechanical and Aerospace Engineering, Institut Teknologi Bandung, Jalan Ganesa, Bandung, Indonesia
[2]Direktorat Teknologi, PT Dirgantara Indonesia,Jl Pajajaran Bandung, Indonesia
E-Mail: mgsuada@gmail.com

## ABSTRACT

A composite laminate is susceptible to Low-Velocity Impact (LVI) load, leading to Barely Visible Impact Damage (BVID) accompanied by invisible damage in the form of delamination. Such delamination is significantly reduced the compression strength of the composite laminate plate. The present work provides an experimental and numerical analysis, based on finite elements, on residual compression strength after the low-velocity impact of carbon/epoxy composite plate. Five specimens of 16 layers Unidirectional carbon/epoxy composite plate with fiber orientation $[+45^0/90^0/-45^0/0^0/+45^0/90^0/-45^0/0^0]$s have been tested subject to low-velocity impact load, with a single use of impact energy value of 2.75 Joule/mm, followed by compression test. Moreover, another similar five specimens tested compression before impact to measure its compression strength. Experimental results were observed to identify the profile and size of total-projection delamination after impact and after compression and compression-strength before and after impact. The Finite Element analysis is based on the utilization of cohesive zone elements with Benzeggagh-Kenane fracture criterion to predict the initiation and propagation of delamination, Kirchhoff based formulation of continuing shell element to model stiffness of the laminate, and Hashim-Rotem damage mechanism to predict intralaminar damages.

**Keywords:** barely visible impact damage, delamination, carbon composite laminate, finite element method (FEM), low-velocity impact (LVI), compression-after impact (CAI), compression-before impact (CBI).

Manuscript Received 7 February 2023; Revised 13 July 2023; Published 25 July 2023

## INTRODUCTION

Low-velocity impact loading leading to a significant compression strength reduction on the composite laminate structure has attracted attention from many researchers; among others are [1], [2], and [3]. The low-velocity impact in composite material creates barely visible impact damage (BVID). Unfortunately, such barely visible impact damage co-exists with invisible damage in the form of delamination. Delamination has a significant contribution to the reduction of compression strength. E.V Gonzalez *et al*. [4] studied the effects of ply clustering on polymer-based laminated composite plates on compression strength reduction subjected to a drop-weight impact loading. The research goal is to find the impact behaviour and the damage threshold that significantly reduces the structural stiffness and compression strength due to delamination. They researched by doing an experimental test on Hexply AS4/8552 carbon epoxy unidirectional pre-preg with different stacking sequences, i.e. $[(45^o/0^o/-45^o/90^o)_4]_s$, $[(45^o{}_2/0^o{}_2/-45^o{}_2/90^o{}_2)_2]_s$, $[(45^o{}_4/0^0{}_4/-45^0{}_4/90^0{}_4)]_s$. They found that the most critical damage in drop weight low-velocity impact is delamination leading to a significant reduction in residual compression strength.

The present paper delivers the results of experimental and numerical approaches to the low-velocity impact analysis of 16 layers Uni-directional (UD) carbon/epoxy composite plate with fiber orientation $[+45^0/90^0/-45^0/+45^0/90^0/-45^0/0^0]$s. Numerical-approach utilizes a cohesive zone element and Benzeggagh-Kenane [5] fracture criterion to predict the initiation and propagation of delamination, Kirchhoff based formulation of continuing shell element to model stiffness of each lamina, and Hashim-Rotem [6] damage mechanism to predict intralaminar damage. An ABAQUS finite element software [10] is used for explicit numerical analysis. The finite element result is then verified to the experimental results. The verification will be executed by comparing the size of total-projection delamination after impact and after compression and strength reduction after compression. The accuracy of predicting compression strength reduction becomes the main interest of the present work.

## TESTING METHODS

The test specimen is made of Hexply AS4/8552 16 layers UD carbon/epoxy composite plate with fiber orientation $[+45^0/90^0/-45^0/+45^0/90^0/-45^0/0^0]_s$. The specimen size and testing methods are ASTM D7136 [7] for low-velocity impact and ASTMD7137 [8] for residual compression strength. Ten specimens have been made and tested, five each for compression test after low-velocity impact and before impact loading test. A single-use of impact energy value of 2.75 Joule/mm is selected. The impact energy is dictated that the damage created is within under classification of BVID as defined in reference [9]. The specimen's thickness ranges between 3.8-3.9 mm, with an average value of 3.84 mm. The low-velocity impact testing was carried out using Impact Drop Weight Impact Testing Machine INSTRON 9350, complying with

ASTM D7136. Moreover, Universal Testing Machine Instron 5982 for a compression test which complies with ASTM D7137.

A TTU machine, manufactured by UltrasonicSciences LTD, has been used to inspect hidden damage such as delamination.

## FINITE ELEMENT MODEL AND MATERIAL PROPERTIES

The mesh in the finite element model is composed of Kirchhoff-based reduced integration continuum shell element SC8R to model stiffness of the lamina and COH3D3 to model a cohesive zone in inter-laminar. Figure-1 below shows the mesh configuration for LVI analysis.

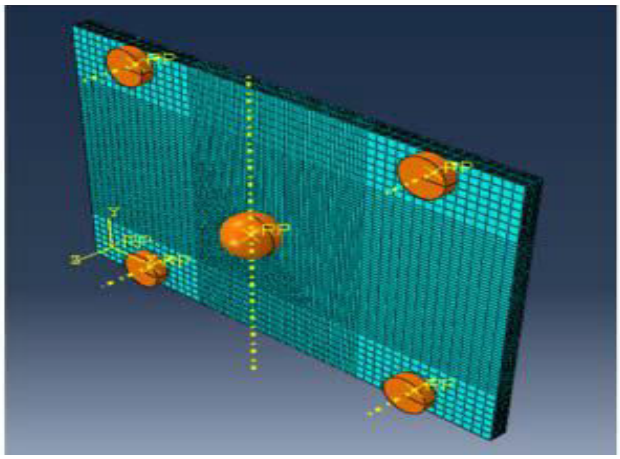

**Figure-1.** Finite Element Model of 16 layers $[+45^0/90^0/-45^0/0^0/+45^0/90^0\ 45^0/0^0]_s$ carbon composite plate subject to low-velocity impact.

In the present work, the authors conduct a finite element sizing following a suggestion from Song [11]. Song suggested that the size of a cohesive element is fine enough to be able to capture the high gradient stress fields near the tips of delamination length (Le) to achieve that is given by $Le = E_i G_{ci}/(N_e S_i^2)$, $Ne \geqq 3$, i=t,n,s. By keeping $G_c$ constant, he wrote that the energy dissipation of the elements is preserved. Furthermore, it is achieved by rearranging the previous equation into $S_i = (E_i G_{ci}/[Ne\ Le])^{0.5}$. Careful calculations lead to size 1.25 mm (length) x 1.25 mm (wide) x 0.23 mm (thick) for SC8R elements and 1.25 mm (length) x 1.25 mm (wide) x 0.006 mm (thick) for COH3D3 elements are adequate. The small element is suggested to be placed in the possible delaminated area. Corser mesh is recommended to be placed outside the damage zone to minimize the number of elements. No-clustering mesh modelling is used in the present model as suggested by reference [12].

To simulate a LVI Finite element model, a boundary condition during low-velocity impact loading, the base plate is modelled as a discrete rigid surface meshed with R3D4 elements. The pins are modelled as analytical rigid body cylinders. The fixture is placed in contact with the laminates with no compressive forces applied to the laminate. Both translation and rotation are constrained in all directions for the fixture. The impactor is modelled as an analytical rigid body sphere with a 0.01 mm distance from the top of the laminate surface with an initial velocity of 2.05 m/s and placed in the middle of the sphere to make impact energy reaches 10.5 Joule. The translation is only permitted in the axis of transverse to the laminate surface. All other translations are constrained. The effect of gravitational acceleration is neglected to ease the energy analysis. Contact between fixtures - laminate and impactor - laminate is defined by the available contact option. A modification of boundary conditions must be taken to simulate a compression loading; including carrying-over damage at intra-laminar and inter-laminar resulted from impact loading analysis. Figure-2 shows modified mesh configuration after LVI analysis for compression strength FEM analysis.

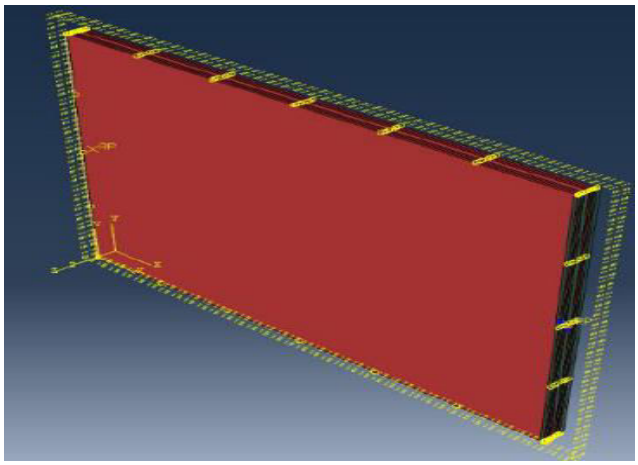

**Figure-2.** Finite Element Model of carbon composite plate subject to compression loading with the out-of-plane fixture at all edges.

Tables 1 and 2 show the material properties of intra-laminar and inter-laminar. The value of transverse shear stiffness ($G_{23}$) assumes that the transverse shear fiber cross-section is isotropic and $\mu_{23} = \mu_{12}$ such that $G_{23}=E_{22}/2(1+\mu_{12})$. The friction coefficient $\mu$ is taken as 0.6. Furthermore, fracture energies ($G_c$) are taken from Gonzales [4]. The properties of Hexply AS4/8552 and cohesive zone interface are taken from [4], [13], and [14] and are shown in Tables 1 and 2.

**Table-1.** Material properties for Hexply AS4/8552.

| Properties | Values |
|---|---|
| Fiber direction stiffness, $E_{11}$ (MPa) | 131610 |
| Transverse fiber direction stiffness, $E_{22}$ (MPa) | 9238. |
| In-plane shear stiffness, $G_{12}$ (MPa) | 4826. |
| Transverse shear stiffness, $G_{13}$ (MPa) | 3548 |
| Longitudinal shear stiffness, $G_{13}$ (MPa) | 4826. |
| In-plane Poisson's ratio, $\mu_{12}$ | 0.302 |
| Density (ton/mm$^3$) | 1.59 x $10^{-9}$ |
| Fiber direction tension strength, $X_T$ (MPa) | 2063. |
| Fiber direction compression strength, $X_C$ (MPa) | 1484. |
| Transverse fiber direction tension strength, $Y_T$ (MPa) | 63. |
| Transverse fiber direction compression tension strength, $Y_C$(MPa) | 267. |
| In-plane shear strength, $S_{12}$ (MPa) | 91. |
| Transverse shear strength, $S_{23}$ (MPa) | 133. |
| $G_{ft}$ Fracture energy fiber direction in tension (N/mm) | 81.5 |
| $G_{fc}$ fiber direction in compression (N/mm) | 106.3 |
| $G_{mt}$ transverse fiber direction in tension (N/mm) | 0.28 |
| $G_{mc}$ transverse fiber direction in compression (N/mm) | 0.79 |

**Table-2.** cohesive zone interface properties.

| Properties | Values |
|---|---|
| Normal stiffness, $k_n$ (MPa/mm) | 36955. |
| Shear stiffness, $k_t$, and $k_s$ (MPa/mm) | 19305. |
| Maximum normal stress, $N_{max}$ (MPa) | 26.26 |
| Maximum shear stress, $S_{max} = T_{max}$ (MPa) | 31.89 |
| Normal fracture energy (N/mm) | 0.28 |
| Shear fracture energy (N/mm) | 0.79 |
| Density, ρ(ton/mm$^3$) | 1.59 x $10^{-9}$ |
| BK mix mode parameter, η | 1.45 |

## DAMAGE EVOLUTION MODEL

The damage evolution mechanism is divided into two folds. The first one is for intra-laminar, and the other one is for inter-laminar. In the intra-laminar, the damage evolution involves predicting damage initiation and evolution in the lamina in the form of matrix tension/compression failure, fiber-direction tension, and compression failures. The Hashin-Roten damage model mechanism has been used for the intra-laminar damage model and Benzeggagh-Kenane for the inter-laminar damage mechanism. A brief description of the damage evolution model for intra-laminar and inter-laminar is described below.

### Intra-laminar Damage Evolution Model

The Hashin-Roten damage model's failure criteria for fiber-reinforced composites have stated four different failure initiations: fiber tension, fiber compression, matrix tension, and matrix compression. The linear softening progressive damage model, as shown in Figure-3, is used.

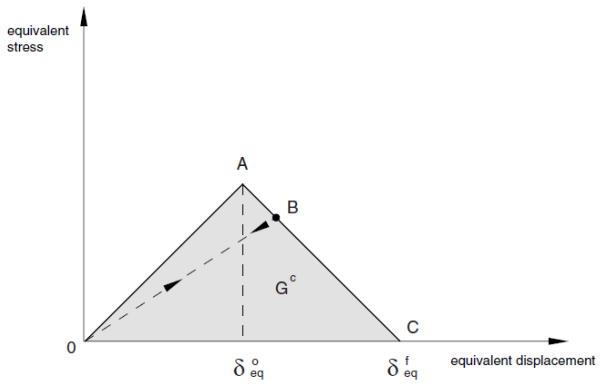


**Figure-3.** Linear softening Progressive Damage model [6].

The stress-strain vector relationship and the constitutive model with linear degradation are formulated as follows:

$$\sigma = C_d \varepsilon \tag{1}$$

$$C_d = \frac{1}{D} \times \begin{bmatrix} (1-d_f)E_1 & (1-d_f)(1-d_m)\nu_{12}E_{12} & 0 \\ (1-d_f)(1-d_m)\nu_{12}E_{12} & (1-d_m)E_2 & 0 \\ 0 & 0 & (1-d_s)GD \end{bmatrix} \tag{2}$$

G is the shear modulus of the lamina, E is the modulus of elasticity, subscript 1 and 2 are in the fiber direction and perpendicular to the fiber direction. And $D$ is:

$$D = 1 - (1-d_f)(1-d_m)\nu_{12}\nu_{21} \tag{3}$$

$d_m$ and $d_f$ are damage scales for matrix and fiber, respectively, and the values follow the progressive linear model as shown in figure 3. When $D$ = 1, the material has lost its load-carrying capacity.

### Inter-laminar Damage Evolution Model

The inter-laminar damage evolution is conducted using the cohesive zone element. The cohesive zone element controls the traction reaction on two attached surfaces and will be detached and expressed by the displacement of the two surfaces. This concept applies if the stress in the axial direction of the field does not exist and the stress is dominated by normal stress and plane

stress only. Possible relative displacements are in the normal / peeling direction and the sliding direction. This displacement also includes traction ($t_n$,$t_s$,$t_t$), which shows the bond resistance between the two surfaces. tn is normal traction, and ts and tt are two perpendicular shear tractions. Traction separation behavior is stated in:

$$\{t\} = [K]\{\varepsilon\} \quad (4)$$

Where {ε} is the separation relative displacement vector (δn,δs,δt in normal and two perpendicular shear directions) and [K] is the cohesive material stiffness matrix. Vector t is the nominal value of traction. The damage initiation in the cohesive zone is assumed to initiate when the quadratic interaction involving the nominal stress ratio reaches one.

$$\left(\frac{t_n}{N_{max}}\right) + \left(\frac{t_s}{S_{max}}\right) + \left(\frac{t_t}{T_{max}}\right) = 1 \quad (5)$$

After the initiation traction failure criteria have been achieved, the component's stiffness experiences softening with a scalar breakdown variable d so that: Where i = t,n,s. variable d varies from 0 to 1, with 1 representing material failure, i.e., material stiffness k reaches 0, as illustrated in Figure-4. The total triangle area in Figure-4 is proportional to critical fracture energy. Therefore, once the condition of fracture reaches its critical value, then delamination is growing.

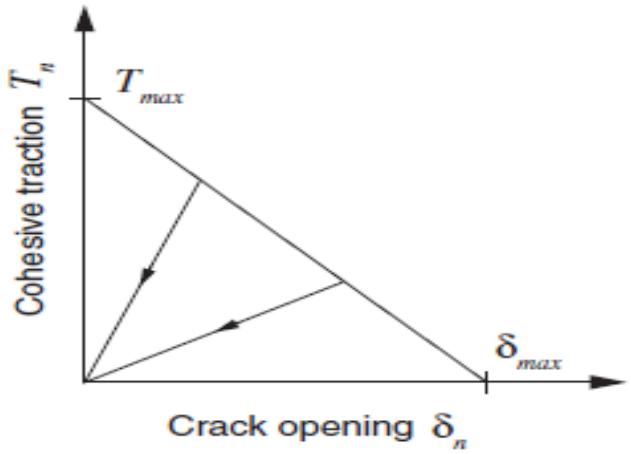


**Figure-4.** Traction-separation response [5].

For mixed-mode cases, the adopted formulation to control delamination progress is the Benzeggagh-Kenane fracture criterion. The proposed formula is as follows: $G_S = Gs + G_t$, $G_T = G_n + G_S$, and η are material parameters.

$$G_n^c + (G_s^c - G_n^c)\left(\frac{G_S}{G_T}\right)^{\eta} = G^c \quad (6)$$

## RESULTS

### Projected Delamination Profile After Impact

Table-3 shows experimental results of projected delamination profile and size after impact loading (LVI)

**Table 3** Projected delamination after impact-Experimental results.

| SPECIMEN ID | | U1 | U2 | U3 | U4 | U5 | Average (mm²) |
|---|---|---|---|---|---|---|---|
| AFTER LVI | Shape | 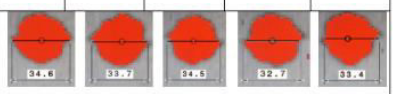 | | | | | |
| | Size (mm²) | 690 | 718 | 708 | 657 | 718 | 698 |

The form of projected delamination after impact is closer to circular for both experimental and numerical FEM results. This is in good agreement with the fact that fiber orientation lay-up configuration is orthotropic. Figure-5 shows the difference of projected delamination profiles between experimental and numerical after low-velocity impact. As we can see that numerical result agrees not only with the experimental one in terms of shape profile but also in terms of size. Table-4 below shows the projected delamination area after LVI, both for experimental (average value) and numerical results. Projected delamination area difference between experimental (average value) and FEM after LVI is 8% less.

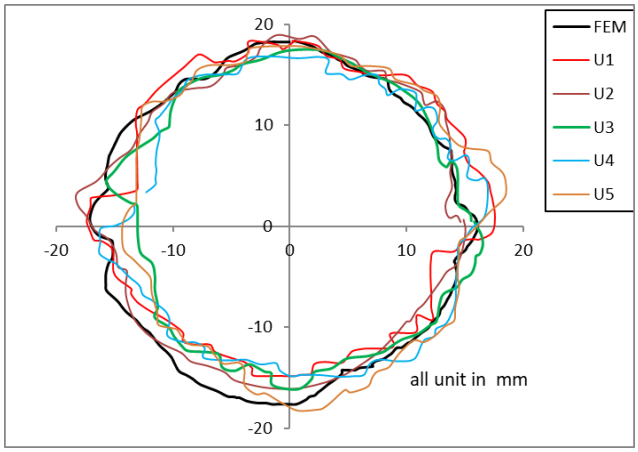


**Figure-5.** Projected delamination profile after Low-Velocity Impact-LVI (Dash line - Experimenta lU1-U5 and solid line FEM).

**Table-4.** Projected delamination comparison (in mm²).

| | Experimental (Average) | FEM | Differences (%) |
|---|---|---|---|
| After LVI | 698 | 720 | 7.8 |

**Residual Compression Strength**

The experimental result (specimen B-1 to B-5) of Compression-Before-Impact in the form of compression stress-strain is depicted in the following figure.

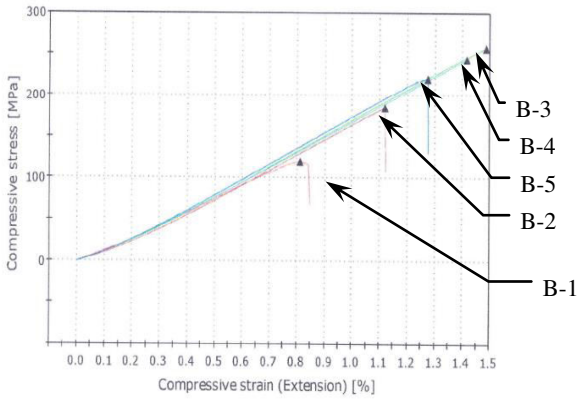


**Figure-6.** Experimental results of Compression-Before-Impact (CBI) for five specimens.

The B-1 data has been excluded since this specimen suffers edge-crushing during the compression test. The TTU result is shown in Figure-7 below.

**Figure-7.** A TTU result of specimen B-1 experiences edge crushing.

The average result for compression before impact is 220 MPa.

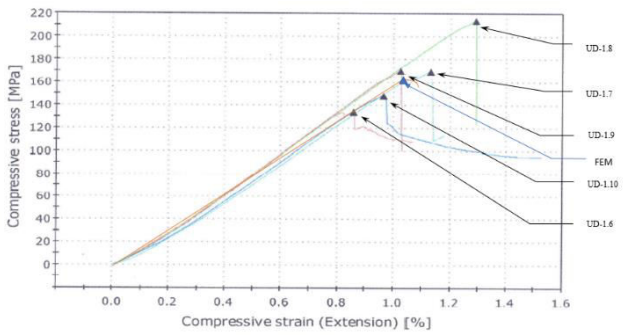


**Figure-8.** Experimental and FEM results of the Compression-After-Impact (CAI).

The average experimental compression strength after LVI is 167 MPa and FEM result is 157 MPa. Figure-9 shows a comparison between experimental results for compression strength before and after Impact and FEM results for CAI.

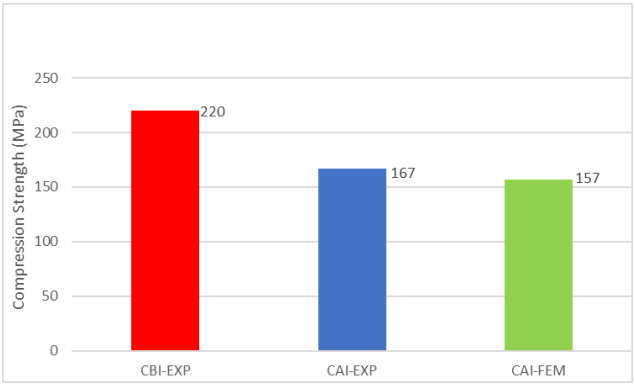


**Figure-9.** Average compression strength before impact-Experimental result (CBI-EXP) in red color, Average after impact-Experimental result (CAI-EXP) in blue color, and After Impact - FEM result in green color (CAI-FEM).

The experimental results show that there is significant compression strength reduction after low-velocity impact. In this case, after experiencing impact energy of 2.75 J/mm, the composite plate has experimentally a 24% compression strength reduction.

This result also confirm the fact that delamination is a significant cause for compression strength reduction, as also revealed in references [1], [2], and [3]. The FEM prediction for residual compression strength after LVI shows a relatively minordifference as compared to the average experimental result, which is in the fraction of less than6%. See Figure-9 above.

## CONCLUSIONS

Experimental and numerical results show that low velocity impact creates invisible damage in the form of delamination which reduce compression strength significantly. In the present cases, the reduction reaches more than 24% after the composite plate impacted by 2.75 J energy.

A FEM analysis which is based on a combination of utilization of cohesive zone element with Benzeggagh-Kenane fracture criterion to model delamination initiation and growth, Kirchhoff based formulation of continuing shell element to model plate stiffness, and Hashim-Rotem damage mechanism achieve a good agreement in predicting delamination and residual compression strength after impact. The residual compression strength difference between experimental and FEMis less than 6%. The FEM analysis is also in a good agreement in predicting shape and size of projected delamination.

## ACKNOWLEDGMENT

The present work is fully funded by Institut Teknologi Bandung through P3MI (Program Penelitian

Pengabdian Masyarakat dan Inovasi) fiscal year 2021. Testing execution and specimen preparations have been provided by PT Dirgantara Indonesia.

**REFERENCES**

[1] S. Sanchez. 2005. Compression after the impact of thin laminates composite laminates. Composites Science and Technology. pp. 1911-1919.

[2] S. Rivallant. 2013. Failure analysis of CFRP laminates subjected to compression after impact: FE simulation using discrete interface elements. Composites: Part A. pp. 83-93.

[3] S. Rivallant. 2013. Experimental analysis of CFRP laminates subjected to compression after impact: The role of impact-induced cracks in failure. Composite Structures. pp. 147-157.

[4] E. V. Gonzalez. 2012. Simulation of drop-weight impact and compression after impact tests on composite laminates. Composite Structures. pp. 3364-3378.

[5] Benzeggagh M.L., Kenane M. 1996. Measurement of mixed-mode delamination fracture toughness of unidirectional glass/epoxy composite with mixed-mode bending apparatus. Composite Science and Technology. 56, 439-449.

[6] Hashin Z., Rotem A. 1973. A fatigue Criterion for fiber-reinforced materials. J. Composite Materials. 7, 448-464.

[7] ASTM D7136, Standard Test Method for Measuring the Damage Resistance of a Fibre-Reinforced Polymer Matrix Composite to a Drop-Weight Impact Event.

[8] ASTM D7137/D7137M - 07. Standard Test Method for Compressive Residual Strength Properties of Damaged Polymer Matrix Composite Plates, December 2007.

[9] Allen J Fawcett. 2006. Composite Airframe Damage Tolerance and service experience, http://www.niar.wichita.edu/chicagoworkshop/Chicago , Damage Tolerance Workshop, July 19-21.

[10] 2011. ABAQUS 6.13 user's manual. Providence (RI, USA): Dassault Systemes Simulia Corp.

[11] Kyongchan Song, Carlos G. Dávila, Cheryl A. Rose. 2008. Guidelines and Parameter Selection for the Simulation of Progressive Delamination. Proceedings of 2008 Abaqus Users' Conference.

[12] S. Abrate. 1998. Impact on composite structures. Cambridge University Press.

[13] NCAMP Test Report Number: CAM-RP-2010_002 Rev A.

[14] Hexply 8552 product datasheet (US), Hexcel Corporation 281 Tresser Boulevard,16th Floor Stamford, CT 06901-3261, USA. (203): 352-6800.